PhotoniX

Laser fabrication of modular superhydrophobic chips for reconfigurable assembly and self-propelled droplet manipulation

Huan Wang[1,2], Yong-Lai Zhang[1*], Dong-Dong Han[1], Wei Wang[1] and Hong-Bo Sun[1,3*]

* Correspondence: yonglaizhang@
jlu.edu.cn; hbsun@tsinghua.edu.cn
[1]State Key Laboratory of Integrated
Optoelectronics, College of
Electronic Science and Engineering,
Jilin University, 2699 Qianjin Street,
Changchun 130012, China
Full list of author information is
available at the end of the article

Abstract

Natural creatures that enables controllable liquid transport provides the inspiration for developing novel microfluidic devices by engineering functional surfaces with superwettability. However, towards microfluidic applications, the strict requirements of sophisticated droplet manipulation make it challenging to reach this end. In this work, we report a conceptually new self-propelled droplet manipulation strategy based on reconfigurable superhydrophobic chips. The modular droplet chip (MDC) is developed by laser embossing a series of superhydrophobic structures on elastomer jigsaws that act as functional units. MDC is potable since only gravity is used as the driving force for dynamic manipulation of liquid droplets, including droplets transporting, splitting, merging and bouncing without mass loss. The MDC demonstrated reasonable anti-cross-contamination property due to the water repellence of the superhydrophobicity. Modular assembly of MDC enables different chip functions including solution dilution, SERS detection, cell labeling and chemical synthesis. As a miniature and portable experimental platform, the MDC is promising for next-generation lab-on-a-chip systems.

Keywords: Superhydrophobic surface, Laser processing, Droplet chip, Droplet manipulation, On-chip analysis

Introduction

As a miniaturized experimental platform, microfluidic chips enable extremely sensitive, efficient, low-consumption, safe and environment-friendly biochemical reactions, revealing great potential in a diverse array of applications ranging from chemical synthesis to biological assays [1–5]. However, with fixed microfluidic channel networks, a given chip is dedicated to a specific reaction, which prevents its practical usage in different assays. More importantly, external auxiliary devices (e.g. pressure pumps for sampling, the microscope for observation, and power sources) significantly limit the portability of such lab-on-a-chip (LoC) systems, making microfluidics a technology for laboratory use only. Recently, in addition to conventional microfluidic chips, some new paradigms, for instance, digital microfluidic (DMF) chips [6–9] and surface-directed

microfluidic (SDMF) systems [10–12], have emerged as alternatives. The former chips are generally reconfigurable for desired combination of droplet operations, since they realize fluidic operations, such as dispensing, transporting, splitting and merging droplets, by electrowetting effect using electrode arrays [13, 14]. The latter chips drive fluids through capillary action of hydrophilic patterns on an open chip, thus they do not require affiliated driving equipment [15, 16]. Although fluid handling can be realized in a controlled fashion, influence from the electric field with respect to DMF chips and the cross-contamination issues of SDMF chips significantly limit their practical applications [17–20]. Therefore, neo microfluidic systems that feature self-controlled fluids handling, reconfigurable channel networks, real portability and extensible functionalities are highly desirable.

In fact, nature creatures have already demonstrated sophisticated capabilities to control small volume liquid, which provides the inspiration for developing novel microfluidic devices [21–23]. For instance, rice leaves control the directional sliding of droplets using anisotropic superhydrophobicity [24, 25]; *Nepenthes* pitcher plants surface enables continuous directional water transport along the peristome surface [26]. These natural phenomena provide a hint that self-controlled liquid transport at microliter-scale can be realized by engineering functional surfaces with unique wettability. However, towards microfluidic chip applications, there are several very strict requirements with respect to droplet manipulation, including energies for driving droplets, directional droplet transport, quantitative droplet splitting and merging, as well as avoiding cross contamination. Consequently, the innovation of nature inspired microfluidic devices that are capable sophisticated droplet manipulation remains a big challenge.

In this work, we report the laser fabrication of modular droplet chips (MDC) that can serve as a reconfigurable, miniature and portable experimental platform for self-propelled droplets manipulations and even on-chip reactions. Gravity is used as the driving force for droplets motion. Flexible manipulation of liquid droplets has been achieved by embossing a series of well-designed 3D superhydrophobic structures on PDMS jigsaws. To endow artificial solid surfaces with desired dewetting properties that are comparable to natural creatures, we embossed superhydrophobic structures including sunken and protuberant morphologies on PDMS slices. To manipulate droplets freely as a chip, we fabricated a series of superhydrophobic embossments on PDMS slices that are designed as modules interlocking with each other, and thus enabling chip functions such as droplets transporting, splitting and merging without mass loss. Flexible assembly of a set of modules achieves different chip functions, for instance, solution dilution, SERS detection, cell labeling and chemical synthesis, revealing great potential for developing next-generation LoC systems.
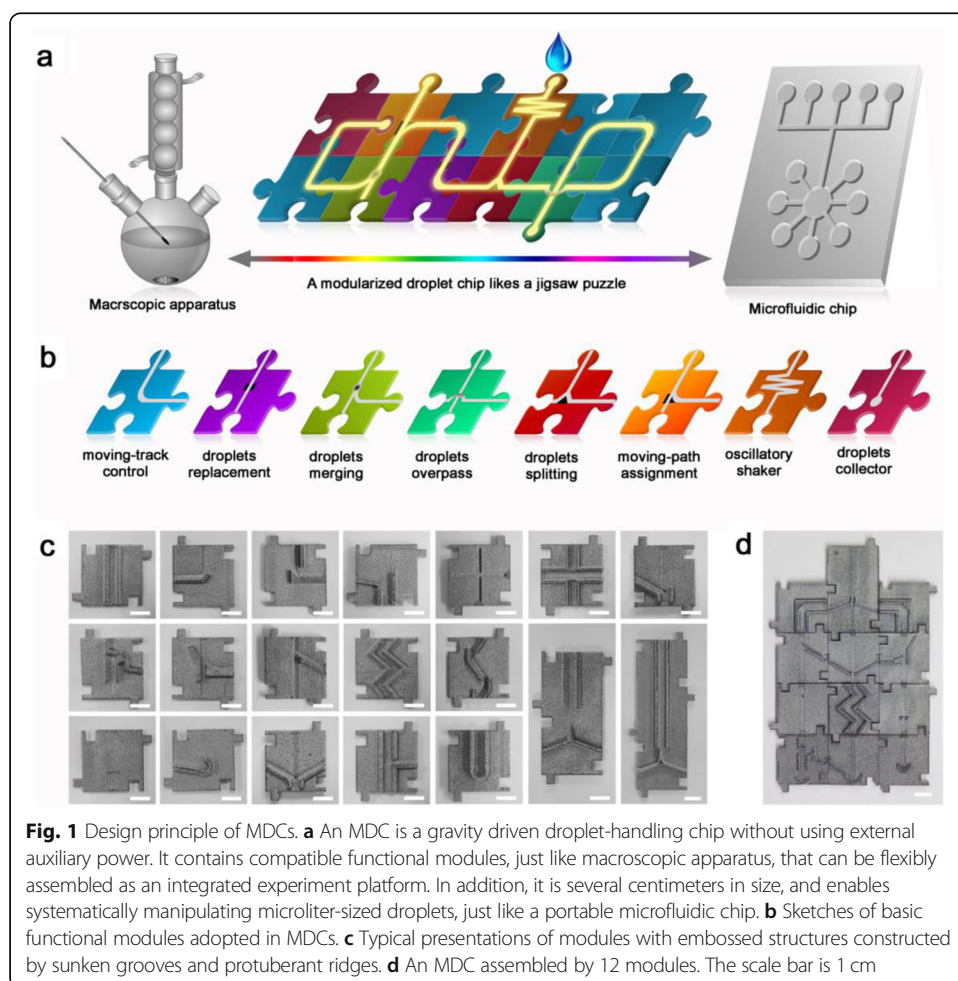
Methods

CO_2 laser with a central wavelength of 10.6 μm is employed for the fabrication. Laser process programs are designed using CorelDRAW. Firstly, embossed structures are engraved on PMMA through subtractive laser manufacturing. Pre-designed structures can be directly created through a layer-by-layer scanning manner. The scanning step length is fixed at 100 μm, and the scanning speed is 100 mm/s. Laser power density is measured to be ~ 6300 W/cm^2. After the subtractive laser manufacturing, embossed structures form on the PMMA surface. The structured PMMA substrate is washed in

water with the help of ultrasonic cleaning, and dried in air for further usage. Secondly, PDMS (contained 10% cross-linking agent, Sylgard 184, Dow Corning) is adopted to duplicate the embossed structures on the PMMA template through a soft lithography process, and cured on a hotplate for 2 h at 80 °C for solidification. In this way, an inverted embossed structure formed on PDMS. Then, another laser treatment is performed to nanotexture the PDMS. In the laser nanotexturing process, the scanning step length is fixed at 100 μm, and the scanning speed is 100 mm/s, the laser power density is 5700 W/cm^2. After laser nanotexturing, the embossed structures become superhydrophobic since the laser treatment introduce micro/nanostructures on PDMS. Finally, a superhydrophobic PDMS chip with embossed functional structures is obtained. To achieve a modular design, the squire chips is a fixed size of 3 × 3 cm, in which a tooth (5 × 5 mm) or a gap (5 × 5 mm) is designed on each side for flexible linkage.
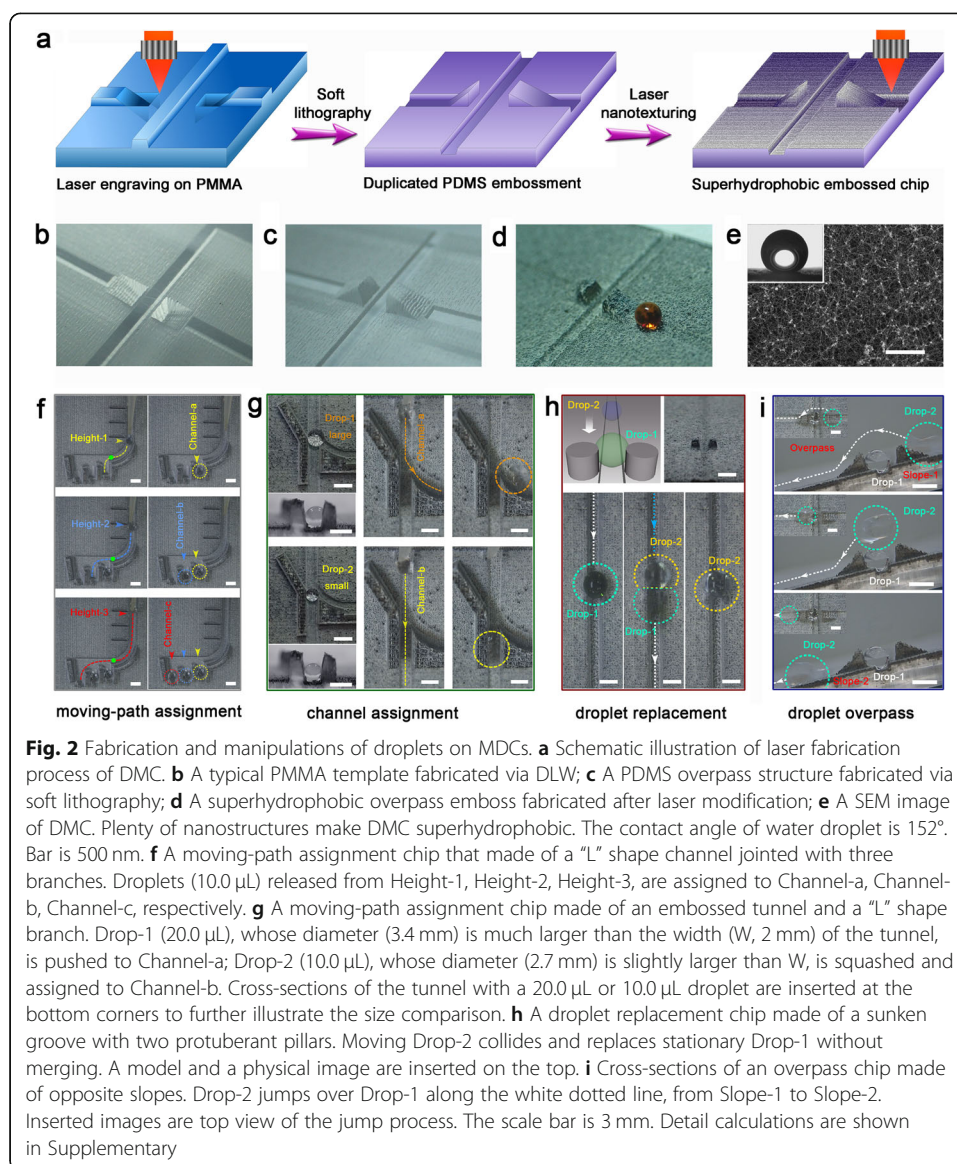
Results and discussion

The design of such MDC aims at bridging the gap between macroscopic apparatus and microfluidic chips (Fig. 1a). Laboratory glassware can be easily assembled into experimental instruments that enable various routine chemical synthesis and analysis. However, their consumption of reagents is between several to hundreds of milliliters, which is a waste of chemicals and a threat to the environment. For microfluidic chips, very

Fig. 1 Design principle of MDCs. **a** An MDC is a gravity driven droplet-handling chip without using external auxiliary power. It contains compatible functional modules, just like macroscopic apparatus, that can be flexibly assembled as an integrated experiment platform. In addition, it is several centimeters in size, and enables systematically manipulating microliter-sized droplets, just like a portable microfluidic chip. **b** Sketches of basic functional modules adopted in MDCs. **c** Typical presentations of modules with embossed structures constructed by sunken grooves and protuberant ridges. **d** An MDC assembled by 12 modules. The scale bar is 1 cm

small dose of reactants (e.g., microliter or even nanoliter scales) is enough, however, microfluidic chips are not reconfigurable, and thus are only specific to a certain experiment. In the case of MDC, only several drops of reagents (one droplet, $5 \sim 150\,\mu L$) are needed for the entire experiments. The MDC not only possesses the advantages of ease of fluid handling without the need of any coupled instruments, but also features the merits of microfluidics, including low reagents consumption, safety, environmental friendliness, high sensitivity and efficiency. To meet the requirements of different experiments, we designed a whole set of chip modules on which different superhydrophobic structures have been embossed for different droplet operations (e.g., moving, replacement, merging, splitting, mixing, and collection of droplets, Fig. 1b). We fabricated the embossed superhydrophobic structures via direct laser writing (DLW). The method enables facile, mask-free and high-efficiency fabrication of large-area superhydrophobic chips with three-dimensional (3D) embossments, thus providing an approach to emboss desired superhydrophobic structures for droplet operation. Figure 1c shows the photographs of different chip modules ($3 \times 3\,cm$ in size), which have been tailored into jigsaw puzzle shapes. The inlet and the outlet of an individual module is fixed at the middle of the sides, thus the assembly of individual modules into a functional chip is very flexible and easy (Fig. 1d). More importantly, the chip is reconfigurable, thus it is suitable for different experiments. Gravity is used as a driving force for droplets operation; thus, no additional instrument is necessary. To convert the gravitational potential energy to kinetic energy, the chips can be tilted at a certain degree. Owning to the surface superhydrophobicity, high energy conversion efficiency can be achieved, which can guarantee a sufficient driving force for droplet operation. The conversion efficiency further depends on the tilted angle and the morphologies of the embossed structures (Supplementary Note 1.1, Fig. S1).

Figure 2a shows the schematic illustration of our fabrication procedures, including laser structuring, soft lithography and laser nanotexturing (see Supplementary materials for methods) [27]. We first embossed an inverse structure as a template on PMMA through subtractive laser manufacturing (Fig. 2b). After that, PDMS is employed to duplicate the embossed structures through a soft lithography process (Fig. 2c). To alter the surface wettability, laser treatment is performed to nanotexture the PDMS, forming the superhydrophobic surface due to the combined effects of carbonization and micronanostructuring (Fig. 2d, e) [28].

To operate a water droplet freely, controlling its moving track is a basic requirement. We designed and fabricated sunken grooves and protuberant ridges, as well as the combination of them to guide droplets transport (Supplementary Movie 1, Supplementary Note 1.2, Fig. S2). Generally, the grooved channel can control the swerving movement of a droplet, providing its moving speed is below 189 mm/s, since the maximum trapping force is calculated to be ~ 23 nN. To guarantee a stable control of high-speed droplet, protuberant ridges structures that can rebound droplets have been embossed. By combining the grooves and the protuberant ridges structures together, more stable droplets delivery can be achieved (Fig. S2d). Besides, as a droplet chip, controllable assignment of the droplet moving path is also very important for droplet delivery. In this work, by embossing special superhydrophobic structures (Supplementary Movie 2, Supplementary Note 1.3), different droplets can be assigned into different channels according to their physical parameters, such as the speed, size, and kinetic energy. We first
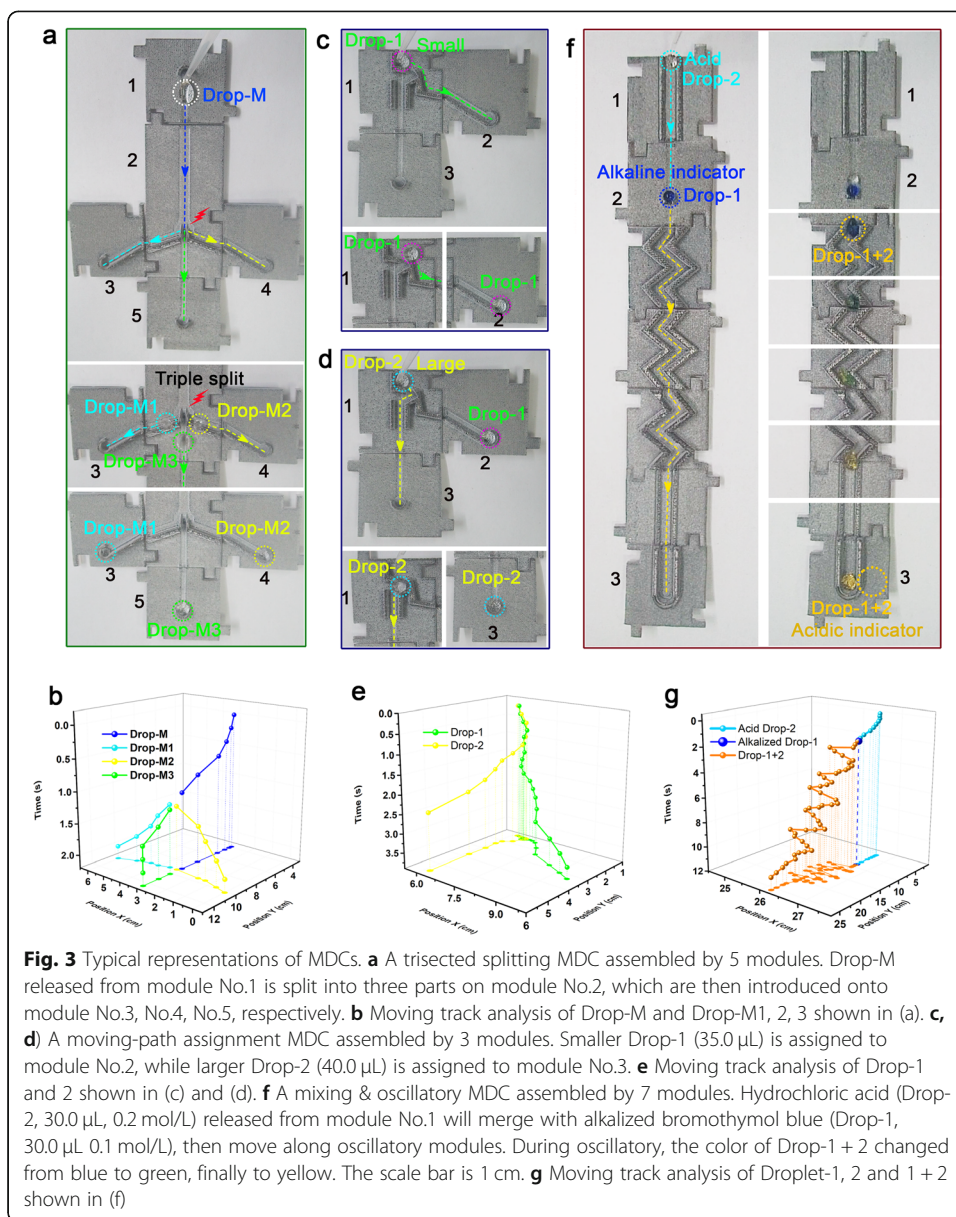
Fig. 2 Fabrication and manipulations of droplets on MDCs. **a** Schematic illustration of laser fabrication process of DMC. **b** A typical PMMA template fabricated via DLW; **c** A PDMS overpass structure fabricated via soft lithography; **d** A superhydrophobic overpass emboss fabricated after laser modification; **e** A SEM image of DMC. Plenty of nanostructures make DMC superhydrophobic. The contact angle of water droplet is 152°. Bar is 500 nm. **f** A moving-path assignment chip that made of a "L" shape channel jointed with three branches. Droplets (10.0 μL) released from Height-1, Height-2, Height-3, are assigned to Channel-a, Channel-b, Channel-c, respectively. **g** A moving-path assignment chip made of an embossed tunnel and a "L" shape branch. Drop-1 (20.0 μL), whose diameter (3.4 mm) is much larger than the width (W, 2 mm) of the tunnel, is pushed to Channel-a; Drop-2 (10.0 μL), whose diameter (2.7 mm) is slightly larger than W, is squashed and assigned to Channel-b. Cross-sections of the tunnel with a 20.0 μL or 10.0 μL droplet are inserted at the bottom corners to further illustrate the size comparison. **h** A droplet replacement chip made of a sunken groove with two protuberant pillars. Moving Drop-2 collides and replaces stationary Drop-1 without merging. A model and a physical image are inserted on the top. **i** Cross-sections of an overpass chip made of opposite slopes. Drop-2 jumps over Drop-1 along the white dotted line, from Slope-1 to Slope-2. Inserted images are top view of the jump process. The scale bar is 3 mm. Detail calculations are shown in Supplementary

demonstrated the assignment droplets with different instant speeds by releasing them at different heights on a titled (10°) chip (Fig. 2f). Droplet released from Height-1, Height-2 and Height-3 can gain an initial speed of ~ 118 mm/s, ~ 201 mm/s and ~ 328 mm/s for the horizontal projectile motions, and thus be assigned to accepting channels of Channel-a, Channel-b and Channel-c, respectively. Droplets moving-path can be also controlled according to their geometry sizes (Fig. 2g). By tuning the width of the embossed tunnel, droplets with different volume can be assigned into different channels. Besides, the moving-path assignment can be also achieved according to the kinetic energy of a droplet (Fig. S3). When a shallow Channel-b jointed with a deep branch Channel-a, a droplet released from different heights at Channel-b will either be trapped in Channel-a or skip over it, which depends on its kinetic energy. The kinetic energy of Drop-3 (trapped in Channel-a) and Drop-4 (skipped over it) is calculated to be 65 and 83 nJ, respectively (at the joint). The above-mentioned structures demonstrate the precise control over the droplet moving-path.
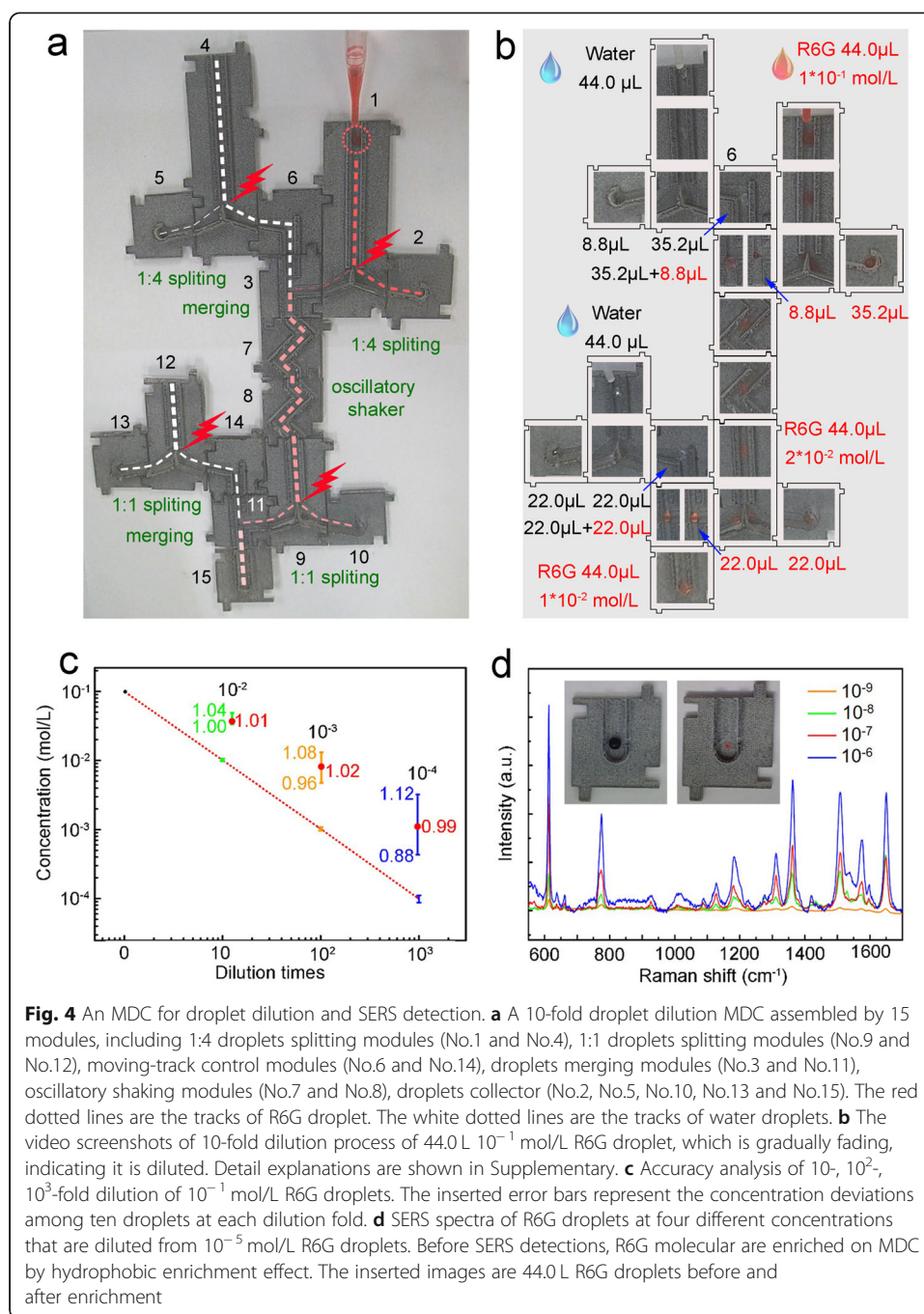
In addition to the droplet movements, splitting, replacing and merging of droplets are also basic functions for droplet chips (Supplementary Movie 3). Splitting droplets accurately enables high-through assays through parallel reactions [29]. By embossing some sharp structures, quantitative droplets splitting can be realized provided the kinetic energy of a droplet is large enough (over 5980 nJ for a 40 µL droplet) to overcome the surface energy (Supplementary Note 1.4, Fig. S4) [30]. Moreover, by tuning the colliding position, it is possible to control the splitting ratio of a droplet, quantitatively (Fig. S4b ~ d, Supplementary Table 1). On the other hand, to operate droplets reactions on a chip, it is necessary to get droplets merged controllably. To reach this end, a droplet can be trapped first, then another moving droplet can be guided to collide and mix with it, and take it away subsequently. A common structure used for droplets merging is the "Y" shape channels including a shallow channel and a deep branch channel (Supplementary Note 1.5, Fig. S5). First, a droplet with relatively small kinetic energy can be trapped at the joint; then another droplet with relatively large kinetic energy will be guided to merge with the trapped droplet and bring it away along the channel. In addition to merging, one droplet would bounce and replace the other one when two droplets meet (Fig. 2h), if the air between them did not have enough time to escape (see Supplementary Note 1.6 for quantitative calculation) [31, 32]. Droplets replacing can be used for sequence reactions.

For 2D microfluidic chips, there exist a limitation that restricts the miniaturization and integration of complex channel networks: two kinds of liquids cannot synchronously pass across a channel junction without mixing. Thus, the channels cannot cross each other. To solve this problem, we designed and fabricated an overpass structure (Fig. 2i, Supplementary Movie 4). By integrating a pair of wedge structures to the channel junction, a droplet can jump over the crossed channel, thus two droplets can pass across the channel without mixing. Such a "overpass" structure would consume ~ 310 nJ of kinetic energy of a droplet (Supplementary Note 1.7, Fig. S6).

By embossing a series of well-designed superhydrophobic structures on one PDMS slice enables on-chip droplet reactions. We demonstrated here the chromogenic reactions (Supplementary Movie 5, Fig. S7). A droplet of pH indicator (Bromothymol Blue) was split into three droplets that fell into different cells, respectively. Then, droplets of acid and alkali released from different channels were guided to mix with each other or directly go to the cells that contained pH indicator. In this way, three chromogenic reactions based on droplets have been realized within several seconds. However, the droplet chip is not reconfigurable. To overcome this limitation, we embossed various superhydrophobic structures as different modules. Flexible assembly of these functional modules can form different chip networks, thus enabling various reactions (Supplementary Movie 6). Figure 3a illustrates a droplet splitting chip assembled through five modules. Two parallel sharp ridges are designed against a groove (module-2), which can quantitatively split Drop-M into three droplets. After the gravity induced accelerating process, the Droplet-M can gain an instantaneous velocity of about 180 m/s in 1 s (blue line, Fig. 3b). When it knocks against the sharp protuberant ridges on module No.2, the droplet was split to three droplets (Drop-M1, 2, 3) that were collected by modules No. 3, 4,5, respectively. Figure 3b records the moving tracks of the as-generated droplets. When these droplets passed the junction between modules, a slight deceleration

Fig. 3 Typical representations of MDCs. **a** A trisected splitting MDC assembled by 5 modules. Drop-M released from module No.1 is split into three parts on module No.2, which are then introduced onto module No.3, No.4, No.5, respectively. **b** Moving track analysis of Drop-M and Drop-M1, 2, 3 shown in (a). **c, d**) A moving-path assignment MDC assembled by 3 modules. Smaller Drop-1 (35.0 µL) is assigned to module No.2, while larger Drop-2 (40.0 µL) is assigned to module No.3. **e** Moving track analysis of Drop-1 and 2 shown in (c) and (d). **f** A mixing & oscillatory MDC assembled by 7 modules. Hydrochloric acid (Drop-2, 30.0 µL, 0.2 mol/L) released from module No.1 will merge with alkalized bromothymol blue (Drop-1, 30.0 µL 0.1 mol/L), then move along oscillatory modules. During oscillatory, the color of Drop-1 + 2 changed from blue to green, finally to yellow. The scale bar is 1 cm. **g** Moving track analysis of Droplet-1, 2 and 1 + 2 shown in (f)

can be detected. Figure 3c, d shows droplets assigning modules. Smaller droplets (Drop-1, < 35 µL) can be assigned to module-2; whereas relative larger droplets (Drop-2, > 40 µL) can be assigned to module-3. The moving track analysis clearly demonstrate the moving-path assignment of the two droplets of different size (Fig. 3e). For chemical reactions, the droplet chip requires merging & oscillatory functions; this can be achieved by assembling a series of groove, merging and oscillatory modules (Fig. 3f). A droplet of hydrochloric acid (Drop-2) was introduced to merge with a droplet of alkalized bromothymol blue (Drop-1) first. Then the merged droplet (Drop-1 + 2) moved along the "Z-shape" oscillatory modules for efficient mixing. Continuous color change from blue to green can be observed due to neutralization reaction. Figure 3g shows the moving track of the droplets, which also reveals their instantaneous velocity at different position.
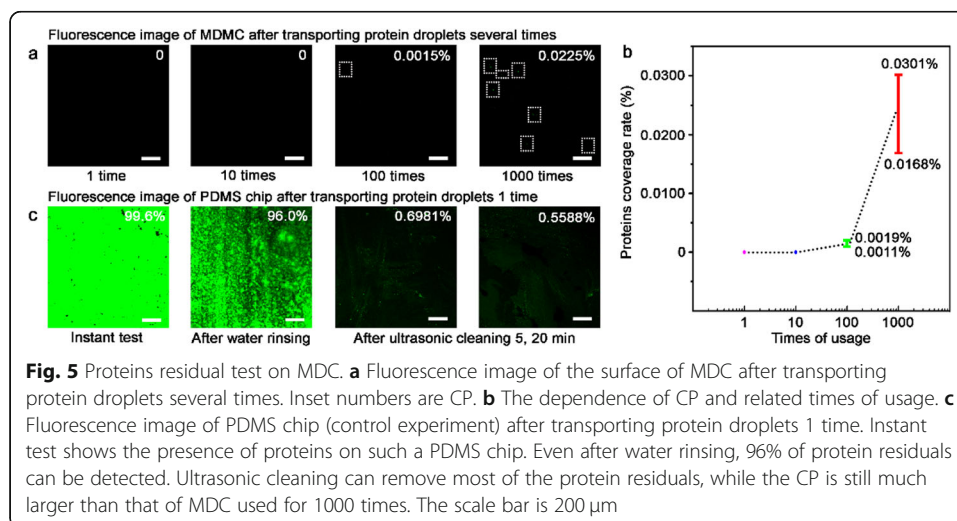
Fig. 4 An MDC for droplet dilution and SERS detection. **a** A 10-fold droplet dilution MDC assembled by 15 modules, including 1:4 droplets splitting modules (No.1 and No.4), 1:1 droplets splitting modules (No.9 and No.12), moving-track control modules (No.6 and No.14), droplets merging modules (No.3 and No.11), oscillatory shaking modules (No.7 and No.8), droplets collector (No.2, No.5, No.10, No.13 and No.15). The red dotted lines are the tracks of R6G droplet. The white dotted lines are the tracks of water droplets. **b** The video screenshots of 10-fold dilution process of 44.0 L 10^{-1} mol/L R6G droplet, which is gradually fading, indicating it is diluted. Detail explanations are shown in Supplementary. **c** Accuracy analysis of 10-, 10^2-, 10^3-fold dilution of 10^{-1} mol/L R6G droplets. The inserted error bars represent the concentration deviations among ten droplets at each dilution fold. **d** SERS spectra of R6G droplets at four different concentrations that are diluted from 10^{-5} mol/L R6G droplets. Before SERS detections, R6G molecular are enriched on MDC by hydrophobic enrichment effect. The inserted images are 44.0 L R6G droplets before and after enrichment

Using these chip modules, more functional chips can be flexibly assembled for different experiments. As a typical example, a 10-fold droplets dilution chip is demonstrated using splitting, moving-path control, merging, oscillatory shaker, and collecting modules (totally 15 modules, Fig. 4a and b, Supplementary Movie 7, Supplementary Note 2.1). A general dropper is employed to inject droplets with an average volume of 44.0 μL on the MDC. The dilution process only requires input one drop of initial solution (R6G aqueous solution) and two drops of water. By repeating this process, 10^2-fold, and 10^3-fold dilution can be achieved. To evaluate the dilution accuracy, the concentrations of the diluted droplets were tested (Fig. 4c). The maximum deviation of

droplets diluted from 10^{-1} mol/L R6G droplets by 10-fold is 4% among ten droplets, and the average concentration is 1.01×10^{-2} mol/L, revealing satisfactory accuracy. In the case of 10^2-fold, and 10^3-fold dilution, the deviations became lager slightly. Nevertheless, the average concentrations are still close to theoretical value. Besides, the concentrations of 10^{-4} mol/L droplets that diluted from 10^{-3}, 10^{-2}, 10^{-1} mol/L R6G droplets, respectively, are also tested (Fig. S8), in which similar dilution accuracy has been achieved (Fig. 4c). The deviations might come from the difference in the volume of individual droplets, the splitting ratio and the evaporation of water, which are inevitable. Even so, such a quantitative droplet dilution chip is promising for real out-lab assays.

Using this MDC, surface enhanced Raman scattering (SERS) experiments can be carried out easily. Typically, R6G droplets of different concentrations diluted above can be easily mixed with a droplet containing silver nanoparticles (AgNPs, Supplementary Note 2.2, Fig. S9). After the evaporation of water, both R6G molecules and AgNPs are enriched on superhydrophobic surfaces within a small region. The aggregation of AgNPs can form abundant "hot spot" under laser irradiation, thus sensitive SERS detection can be realized (Fig. 4d) [33]. The superhydrophobicity is quite helpful for the enrichment of analytes. By using superhydrophobic surface to control concentration, much high sensitivities are achievable [34]. On the other hand, to avoid the evaporation of solvents during long time experiments, ionic liquids can be used instead of water. As a typical example, the polymerization reaction of aniline was carried out based on this MDC (Supplementary Note 2.3, Fig. S10) [35].

In addition, MDC could be used in biology research (Supplementary Note 2.4, Fig. S11). Biomolecular, especially proteins, are easily adsorbed by the solid surfaces, which is a serious issue that limits the practical applications of DMF [36]. Superhydrophobic surfaces could prevent protein adsorption effectively due to the presence of a thin air layer between the droplets and the solid substrate [20]. To confirm this hypothesis, droplets that contain high concentration of anti-human IgG (whole molecule)-FITC were released to move on a superhydrophobic MDC (Supplementary Note 2.5, Fig. 5), then the labeled and unlabeled areas (A_1 and A_2) of the MDC were identified from

Fig. 5 Proteins residual test on MDC. **a** Fluorescence image of the surface of MDC after transporting protein droplets several times. Inset numbers are CP. **b** The dependence of CP and related times of usage. **c** Fluorescence image of PDMS chip (control experiment) after transporting protein droplets 1 time. Instant test shows the presence of proteins on such a PDMS chip. Even after water rinsing, 96% of protein residuals can be detected. Ultrasonic cleaning can remove most of the protein residuals, while the CP is still much larger than that of MDC used for 1000 times. The scale bar is 200 μm

fluorescence images to calculate protein coverage rate (CR, $\frac{A_1}{A_1+A_2} \times 100\%$). Notably, no fluorescence signals can be detected on the MDC after transporting protein droplets for 10 times, demonstrating good antipollution capability. Even after transporting the droplets for 1000 times, the protein CR is only 0.0225%. On the contrary, for general PDMS chip without superhydrophobic modifications, considerable proteins residual can be observed after only once transport of a protein droplet. According to these results, MDC that features antipollution property could effectively reduce the biomolecular residual, emerging as a reusable experimental platform for biochemical reactions [37, 38].

From a practical perspective, currently available microfluidic devices suffer from the limitations with respect to suitability for different reactions, cross-contamination in reuse and the necessary external auxiliary equipment. For conventional microfluidic chips with fixed microfluidic channel network, a chip is generally dedicated to a specific reaction, which lacks general applicability in different analysis. For emerging DMF and SDMF chips, the issue of cross-contamination is ineluctable, which also restricts practical usage. More importantly, most of the microfluidic chips themselves are miniature devices with small dimension and portability. Nevertheless, the use of microfluidic chips usually involves complex external auxiliary equipment, for instance, pumps and microscope. All of the above-mentioned limitations make microfluidics a technology for laboratory use only. And therefore, it is highly desirable to develop neo microfluidic systems that can address these issues.

Conclusions

Herein, inspired by the droplets transport on natural micro/nanostructures, we designed and fabricated MDC that permit flexible manipulation of various droplets by embossing superhydrophobic structures including sunken and protuberant morphologies on PDMS slices. Gravity has been used as a driving force, accurate droplets operations including droplets transporting, splitting, merging, replacing, jumping, oscillating, and collecting have been realized without the use of any couple instruments. The resultant superhydrophobic PDMS modules can be assembled into functional droplet chips for various experiments. Bearing a modular design, the chip is reconfigurable. Using MDCs, common experiments, such as biological label, optical detection, solution dilution, and chemical synthesis, can be realized. By taking advantage of the superhydrophobicity, reagents residual can be avoided, thus the chip modules are reusable. The MDC features controllable fluids handling, reconfigurable chips structures, portability and extensible functionalities, revealing great potential for the next generation of lab-on-chip systems.

Supplementary Information

The online version contains supplementary material available at https://doi.org/10.1186/s43074-021-00033-1.

Additional file 1: Fig. S1. Five cross-sections of representative grooves employed in DMC. The droplets are 10.0 μL. Cross-sections of groove a, b, c are triangles; d, e, are trapezoids. The contact areas between droplets and grooves increase when θ or d deceases, which directly influence the energy transferring of droplets on DMC. Bar is 1.5 mm. **Fig. S2.** a, a serpentine groove for multidirectionally transporting a droplet. b, a curve groove chip designed for testing the threshold situation of derailing. Drop-8 released from Height-8 smoothly passes the channel, while Drop-9 input from Height-9 derails. c, a ridge array chip can transport a droplet through rebounding. d, a droplet transporting chip that combines grooves and ridges. e, a circle ridge module can realize more stable droplets delivery even at high speed. Bar is 4 mm. **Fig. S3.** A droplets moving-path assignment chip: a shallow straight Channel-b with a deep branch Channel-a. The chip is tilted 13°. Droplets released from Height-2, − 3, are assigned

to Channel-a. Droplets released from height-4, − 5 are assigned to Channel-b. Bar is 5 mm. **Fig. S4.** a, droplets splitting module. Only droplets released from Height-9 or above can be split. b, c, d, if droplets are released at Height-9, D_n decides droplets split ratios. D_n is the distance between the end of the curve ridge and the split ridge; D_1, D_2, D_3, are 10.5, 7.5, 3.5 mm, respectively. The split ratios are about 20.0:20.0, 27.5:12.5, 33.9:6.1, respectively. More tests please see Table S1. Bar is 5 mm. **Fig. S5.** Droplets merging & mixing module. a, design scheme. b, an optical image of the merging component. c, merging and mixing process of drop-1 and drop-2. Bar is 5 mm. **Fig. S6.** a, an overpass MDC; the length of the channel from start point to end point is 6 cm. b, magnified image of the overpass in a. c, magnified image of the interface in a. d, a module with flat channel; the length of the channel from start point to end point is 6 cm. Bar in a and d is 1 cm. Bar in a and d is 0.5 cm. **Fig. S7.** An integrated chromogenic reaction chip, which contains pH indicator (1), acid (2), alkali (3), three input ports. a, dark green bromothymol blue Drop-1 is released from Port-1, then is split twice to three parts which are introduced to reaction Cell-1, Cell-2, Cell-3, respectively. b, 10.0 μL 0.1 mol/L hydrochloric acid Drop-2 is input from Port-2, then encounters a moving-path assignment component, and is assigned to a trapping well of a merging component; 10.0 μL 0.1 mol/L sodium hydroxide Drop-3 is input from Port-3, then is assigned to the above-mentioned merging component, merging and neutralizing with hydrochloric acid Drop-2. The merging droplet continuously collides with ridges on sides to promote the reaction, finally moves to Cell-1. Because of the equivalent and thorough neutralization reaction, the pH indicator in Cell-1 does not discolor. c, 50.0 μL 0.1 mol/L hydrochloric acid Drop-4 is released from Port-2, then is assigned to yellow dash marked path due to large size, jumps over a ridge, reaches Cell-2, eventually leads pH indicator discoloring to be yellow. d, 40.0 μL 0.1 mol/L sodium hydroxide Drop-5 is released from Port-3, then is assigned to the blue marked path, merges with pH indicator in Cell-3 and alkalify it to be blue. Totally, droplets moving-track control, splitting, moving-path assignment, merging, overpass, oscillatory shaker, and collector components are integrated on one chip. Bar is 1 cm. **Fig. S8.** Concentration test of droplets 10-fold diluted from 10^{-3} mol/L R6G droplets. The average concentration is 1.01×10^{-4} mol/L, and the largest deviations are 4% from 10^{-4} mol/L R6G standard solution among ten droplets. Similarly, the average concentration of droplets 10^2-fold, 10^3-fold diluted from 10^{-2} mol/L, 10^{-1} mol/L droplets, is 0.99×10^{-4} mol/L, 0.98×10^{-4} mol/L; the largest deviations are 8%, 15% from 10^{-4} mol/L R6G standard solution among ten droplets, respectively. **Fig. S9.** a, Transmission electron microscope image of triangular Ag nanoplates. Bar is 100 nm. Insert is high resolution transmission electron microscope image of a triangular Ag nanoplate. Bar is 20 nm. b, optical image of aggregated Ag nanoplates absorbed with R6G molecules, which is left from the mixture of 22 μL 1 mg/ml Ag NPs and 22 μL 10^{-6} mol/L R6G solution. SERS spectrums are collected on the aggregated substrates. Bar is 200 nm. **Fig. S10.** a, optical images of the ionic liquid droplet reaction during the polymerization, shown in b. The color turns to be black from transparent after tens of minutes, while the contact angles are still large than 142° (insert images). Bar is 1 cm. c, SEM image of the synthesized polyaniline, which is similar with a related literature. Bar is 500 nm. **Fig. S11.** a, the collector module of cell labeling chip. It is selectively laser nanotextured, leaving an area of transparent PDMS that allows to directly observe cells on the chip under microscope. Bar is 1 cm. b, optical and fluorescence image of the labeled MCF-7. Bar is 20 μm. **Supplementary Table 1.** Test results of splitting module in Fig. S4. Initial droplets are 40.0 μL, and released from graduation 9. The splitting ratios depends on DX. The splitting deviations are smaller than 0.1 μL. (DOCX 4259 kb)

Additional file 2: Supplementary Movie 1. Moving-track control chips: a serpentine groove chip for multidirectional transporting a droplet; droplet derailing threshold test of a "L" shape chip; a ridge array chip transports a droplet through rebounding; a droplet transporting chip combines grooves and ridges; a circle ridge chip transports a droplet in almost 360°. (AVI 10464 kb)

Additional file 3: Supplementary Movie 2. Moving-path assignment chips: a chip that assigns droplets by instant speeds; a chip that assigns droplets by geometry sizes; a chip that assigns droplets by kinetic energy. (AVI 6086 kb)

Additional file 4: Supplementary Movie 3. Droplets splitting threshold test; droplets multi-ratio splitting chips; droplets merging chips; droplets replacement chips. (AVI 9278 kb)

Additional file 5: Supplementary Movie 4. Side and top views of an overpass chip, which enables two droplets passing across the channel without mixing. (AVI 3306 kb)

Additional file 6: Supplementary Movie 5. An integrated chromogenic reaction chip that combines droplets moving-track control, droplets merging, droplets overpass, droplets splitting, moving-path assignment, oscillatory shaker, droplets collector functions in one chip. (AVI 2199 kb)

Additional file 7: Supplementary Movie 6. A trisected splitting MDC; a moving-path assignment MDC; a merging & oscillatory MDC; a cell labeling MDC. (AVI 2542 kb)

Additional file 8: Supplementary Movie 7. A droplet dilution MDC assembled by 15 modules. One droplet of R6G aqueous solution is firstly input onto the chip, then two droplets of water are input. As a result, a 10-fold dilution R6G droplet is obtained. (AVI 1452 kb)

Availability of data and materials
The data that support the findings of this study are available from the corresponding author on request.

Declarations

Competing interests
The authors declare that they have non-financial competing interests.

Author details
[1]State Key Laboratory of Integrated Optoelectronics, College of Electronic Science and Engineering, Jilin University, 2699 Qianjin Street, Changchun 130012, China. [2]Hooke Instruments, Changchun Institute of Optics, Fine Mechanics and Physics, Chinese Academy of Sciences, Changchun 130033, China. [3]State Key Laboratory of Precision Measurement Technology and Instruments, Department of Precision Instrument, Tsinghua University, Haidian, Beijing 100084, China.

References

1. Hol FJH, Dekker C. Zooming in to see the bigger picture: microfluidic and nanofabrication tools to study bacteria. Science. 2014;346:438.
2. Demello AJ. Control and detection of chemical reactions in microfluidic systems. Nature. 2006;442(7101):394–402. https://doi.org/10.1038/nature05062.
3. Yager P, Edwards T, Fu E, Helton K, Nelson K, Tam MR, et al. Microfluidic diagnostic technologies for global public health. Nature. 2006;442(7101):412–8. https://doi.org/10.1038/nature05064.
4. Craighead H. Future lab-on-a-chip technologies for interrogating individual molecules. Nature. 2006;442(7101):387–93. https://doi.org/10.1038/nature05061.
5. Wang H, Zhang YL, Wang W, Ding H, Sun HB. On-chip laser processing for the development of multifunctional microfluidic chips. Laser Photonics Rev. 2017;11(2):1600116. https://doi.org/10.1002/lpor.201600116.
6. Ng AHC, Chamberlain MD, Situ H, Lee V, Wheeler AR. Digital microfluidic immunocytochemistry in single cells. Nat Commun. 2015;6(1):7513. https://doi.org/10.1038/ncomms8513.
7. Ottesen EA, Hong JW, Quake SR, Leadbetter JR. Microfluidic digital PCR enables multigene analysis of individual environmental bacteria. Science. 2006;314(5804):1464–7. https://doi.org/10.1126/science.1131370.
8. Tadmor AD, Ottesen EA, Leadbetter JR, Phillips R. Probing individual environmental bacteria for viruses by using microfluidic digital PCR. Science. 2011;333(6038):58–62. https://doi.org/10.1126/science.1200758.
9. Abdelgawad M, Wheeler AR. The digital revolution: a new paradigm for microfluidics. Adv Mater. 2009;21(8):920–5. https://doi.org/10.1002/adma.200802244.
10. Zhao B, Moore JS, Beebe DJ. Surface-directed liquid flow inside microchannels. Science. 2001;291(5506):1023–6. https://doi.org/10.1126/science.291.5506.1023.
11. Zahner D, Abagat J, Svec F, Fréchet JMJ, Levkin PA. A facile approach to superhydrophilic-superhydrophobic patterns in porous polymer films. Adv Mater. 2011;23(27):3030–4. https://doi.org/10.1002/adma.201101203.
12. You I, Kang SM, Lee S, Cho YO, Kim JB, Lee SB, et al. Polydopamine microfluidic system toward a two-dimensional, gravity-driven mixing device. Angewandte Chemie-Int Ed. 2012;51(25):6126–30. https://doi.org/10.1002/anie.201200329.
13. Srinivasan V, Pamula VK, Fair RB. An integrated digital microfluidic lab-on-a-chip for clinical diagnostics on human physiological fluids. Lab Chip. 2004;4(4):310–5. https://doi.org/10.1039/b403341h.
14. Cho SK, Moon HJ, Kim CJ. Creating, transporting, cutting, and merging liquid droplets by electrowetting-based actuation for digital microfluidic circuits. J Microelectromech Syst. 2003;12:70–80.
15. Zhao B, Moore JS, Beebe DJ. Principles of surface-directed liquid flow in microfluidic channels. Anal Chem. 2002;74(16):4259–68. https://doi.org/10.1021/ac020269w.
16. Yang SY, Defranco JA, Sylvester YA, et al. Integration of a surface-directed microfluidic system with an organic electrochemical transistor array for multi-analyte biosensors. Lab Chip. 2009;9(5):704–8. https://doi.org/10.1039/B811606G.
17. Choi K, Ng AHC, Fobel R, et al. Digital microfluidics, cooks R G, Yeung E S, editor, annual review of analytical chemistry, Vol 5, Palo Alto: Annual Reviews; 2012. p. 413–40.
18. Bouaidat S, Hansen O, Bruus H, Berendsen C, Bau-Madsen NK, Thomsen P, et al. Surface-directed capillary system; theory, experiments and applications. Lab Chip. 2005;5(8):827–36. https://doi.org/10.1039/b502207j.
19. Genzer J, Efimenko K. Recent developments in superhydrophobic surfaces and their relevance to marine fouling: a review. Biofouling. 2006;22(5):339–60. https://doi.org/10.1080/08927010600980223.
20. Ng AHC, Li BB, Chamberlain MD, et al. Digital microfluidic cell culture, Yarmush M L, editor, annual review of biomedical engineering, Palo Alto: Annual Reviews; 2015. p. 91–112.
21. Zheng YM, Bai H, Huang ZB, et al. Directional water collection on wetted spider silk. Nature. 2010;463(7281):640–3. https://doi.org/10.1038/nature08729.
22. Parker AR, Lawrence CR. Water capture by a desert beetle. Nature. 2001;414(6859):33–4. https://doi.org/10.1038/35102108.
23. Liu KS, Yao X, Jiang L. Recent developments in bio-inspired special wettability. Chem Soc Rev. 2010;39(8):3240–55. https://doi.org/10.1039/b917112f.
24. Bixler GD, Bhushan B. Fluid drag reduction and efficient self-cleaning with rice leaf and butterfly wing bioinspired surfaces. Nanoscale. 2013;5(17):7685–710. https://doi.org/10.1039/c3nr01710a.
25. Bixler GD, Bhushan B. Bioinspired rice leaf and butterfly wing surface structures combining shark skin and lotus effects. Soft Matter. 2012;8(44):11271–84. https://doi.org/10.1039/c2sm26655e.
26. Chen HW, Zhang PF, Zhang LW, et al. Continuous directional water transport on the peristome surface of Nepenthes alata. Nature. 2016;532(7597):85–9. https://doi.org/10.1038/nature17189.

27. Yong JL, Yang Q, Chen F, et al. A simple way to achieve superhydrophobicity, controllable water adhesion, anisotropic sliding, and anisotropic wetting based on femtosecond-laser-induced line-patterned surfaces. J Mater Chem A. 2014; 2(15):5499–507. https://doi.org/10.1039/C3TA14711H.

28. Wang W, Liu YQ, Liu Y, Han B, Wang H, Han DD, et al. Direct laser writing of superhydrophobic PDMS elastomers for controllable manipulation via Marangoni effect. Adv Funct Mater. 2017;27(44):1702946. https://doi.org/10.1002/adfm.201702946.

29. Dong C, Jia YW, Gao J, et al. A 3D microblade structure for precise and parallel droplet splitting on digital microfluidic chips. Lab Chip. 2017;17(5):896–904. https://doi.org/10.1039/C6LC01539E.

30. Mertaniemi H, Jokinen V, Sainiemi L, Franssila S, Marmur A, Ikkala O, et al. Superhydrophobic tracks for low-friction, guided transport of water droplets. Adv Mater. 2011;23(26):2911–4. https://doi.org/10.1002/adma.201100461.

31. Mertaniemi H, Forchheimer R, Ikkala O, Ras RHA. Rebounding droplet-droplet collisions on superhydrophobic surfaces: from the phenomenon to droplet logic. Adv Mater. 2012;24(42):5738–43. https://doi.org/10.1002/adma.201202980.

32. Yi N, Huang B, Dong LN, et al. Temperature-induced coalescence of colliding binary droplets on superhydrophobic surface. Sci Rep. 2014;4:4303.

33. Chou SY, Yu CC, Yen YT, Lin KT, Chen HL, Su WF. Romantic story or raman scattering? Rose petals as ecofriendly, low-cost substrates for ultrasensitive surface-enhanced raman scattering. Anal Chem. 2015;87(12):6017–24. https://doi.org/10.1021/acs.analchem.5b00551.

34. Pavliuk G, Pavlov D, Mitsai E, et al. Ultrasensitive SERS-based plasmonic sensor with analyte enrichment system produced by direct laser writing. Nanomaterials. 2020;10:49.

35. Zhou Z, He DL, Guo YN, et al. Photo-induced polymerization in ionic liquid medium: 1. Preparation of polyaniline nanoparticles. Polym Bull. 2009;62(5):573–80. https://doi.org/10.1007/s00289-009-0038-y.

36. Malic L, Brassard D, Veres T, Tabrizian M. Integration and detection of biochemical assays in digital microfluidic LOC devices. Lab Chip. 2010;10(4):418–31. https://doi.org/10.1039/B917668C.

37. Koc Y, De Mello AJ, Mchale G, et al. Nano-scale superhydrophobicity: suppression of protein adsorption and promotion of flow-induced detachment. Lab Chip. 2008;8(4):582–6. https://doi.org/10.1039/b716509a.

38. Sun TL, Tan H, Han D, et al. No platelet can adhere - largely improved blood compatibility on nanostructured superhydrophobic surfaces. Small. 2005;1(10):959–63. https://doi.org/10.1002/smll.200500095.

Publisher's Note

Springer Nature remains neutral with regard to jurisdictional claims in published maps and institutional affiliations.